Dipolar interaction in ultra-cold atomic gases

C. Menotti[*], M. Lewenstein[†], T. Lahaye[**] and T. Pfau[**]

[*]*ICFO – Institut de Ciències Fotòniques, E-08860 Castelldefels, Barcelona, Spain*
and CNR-INFM-BEC and Dipartimento di Fisica, Università di Trento, I-38050 Povo, Italy
[†]*ICFO – Institut de Ciències Fotòniques, E-08860 Castelldefels, Barcelona, Spain*
and ICREA – Institució Catalana de Recerca i Estudis Avançats, E-08010 Barcelona, Spain
[**]*5. Physikalisches Institut, Universität Stuttgart, D-70550 Stuttgart, Germany*

Abstract. Ultra-cold atomic systems provide a new setting where to investigate the role of long-range interactions. In this paper we will review the basics features of those physical systems, in particular focusing on the case of Chromium atoms. On the experimental side, we report on the observation of dipolar effects in the expansion dynamics of a Chromium Bose-Einstein condensate. By using a Feshbach resonance, the scattering length characterising the contact interaction can be strongly reduced, thus increasing the relative effect of the dipole-dipole interaction. Such experiments make Chromium atoms the strongest candidates at present for the achievement of the strong dipolar regime. On the theoretical side, we investigate the behaviour of ultra-cold dipolar systems in the presence of a periodic potential. We discuss how to realise this situation experimentally and we characterise the system in terms of its quantum phases and metastable states, discussing in detail the differences with respect to the case of zero-range interactions.

1. INTRODUCTION: ULTRA-COLD ATOMIC SYSTEMS

The cooling and trapping techniques for neutral atoms developed in the last 20 years have allowed the achievement of Bose-Einstein condensation [1], quantum degenerate Fermi gases [2], and the creation of several kinds of correlated systems. In all those cases, a crucial role is played by the statistics of the atoms, the interatomic interactions, the geometry of the system and their interplay.

The first experiments were carried out with ultra-cold bosons in the weakly interacting regime, where the Gross-Pitaevskii equation provides a good description of the system. Due to the very low temperature in those systems, interactions are usually s-wave and hence well described by a zero-range contact potential. Within the Gross-Pitaevskii theory, a huge variety of phenomena has been described, like collective oscillations [3], interference [4] and coherence effects [5], non linear atom optics (4-wave mixing [6] and solitons [7]), superfluidity (sound propagation [8], scissor modes [9], and quantised vortices [10]). In polarised (single species) fermionic systems s-wave interactions are forbidden due to the Pauli principle, so that interactions are normally introduced by considering two different internal sublevels, mixtures of different species or p-wave interactions.

By increasing the strength of the interactions (e.g. by enhancing the scattering length via Feshbach resonances [11]) or by changing the dimensionality of the system, correlations can be introduced. Striking examples in this direction were the observation of the superfluid to Mott insulator transition in optical lattices [12] and the Berezinskii-Kosterlitz-Thouless transition [13], the realisation of a Tonks-Girardeau gas [14], the

study of the BCS-BEC crossover in fermionic systems [15] and the creation of ultra-cold molecules [16].

A further possibility is to consider atoms interacting via long-range dipolar interactions [17]. This will be the topic of this paper, which summarises the talks given at the conference *Dynamics and thermodynamics of systems with long range interaction: theory and experiments* (Assisi, Italy – July 2007) by Chiara Menotti from ICFO, Barcelona and Tobias Koch from the group of Tilman Pfau at the University of Stuttgart. We will explain how long-range interactions arise in ultra-cold atomic systems, and in particular present the observation of weak and strong dipolar interactions in a degenerate sample of Chromium atoms. Moreover, we will discuss the effect of dipolar interactions on atoms trapped in an optical lattice and point out the striking differences with respect to the case of zero-range interactions. The most recent experimental and theoretical results presented here are contained respectively in our papers [18, 19].

For the interested reader, extensive reviews on the physics of ultra-cold bosonic and fermionic ultra-cold gases can be found in [20, 21, 22, 23, 24].

2. INTERATOMIC INTERACTIONS

Although ultra-cold gases have extremely low densities (typically below 10^{15} cm^{-3}), their properties are strongly influenced by interactions [20, 21, 22]. Usually, only the short range, isotropic *contact* interaction plays a role in quantum degenerate gases. However, another type of interaction, namely the anisotropic, long range interaction between dipolar particles, has attracted a lot of interest recently [17].

2.1. Contact potential

In the ultra-low temperature regime relevant for quantum-degenerate gases, scattering occurs only in the s-wave regime, as the centrifugal barrier for other partial waves is much higher than the typical kinetic energies of the atoms. A consequence of this fact is that the real, complicated interatomic molecular potentials (which at long distances are essentially given by Van der Waals attraction $-C_6/r^6$) can be replaced for most purposes by a simple, isotropic and short-range model potential proportional to the scattering length a of the atoms. This *contact interaction* reads

$$U_{\text{contact}}(\mathbf{r}) = \frac{4\pi\hbar^2 a}{m}\delta(\mathbf{r}) \equiv g\delta(\mathbf{r}),$$

(1)

where m is the atomic mass. Most of the interesting properties observed in quantum gases since the first observation of BEC in dilute atomic vapours in 1995 can be understood by using this simple interatomic potential.

2.2. Dipole dipole interaction (DDI) potential

Atoms or molecules having a permanent dipole moment (either magnetic or electric) interact not only via short-range potentials, but also via the dipole-dipole interaction.
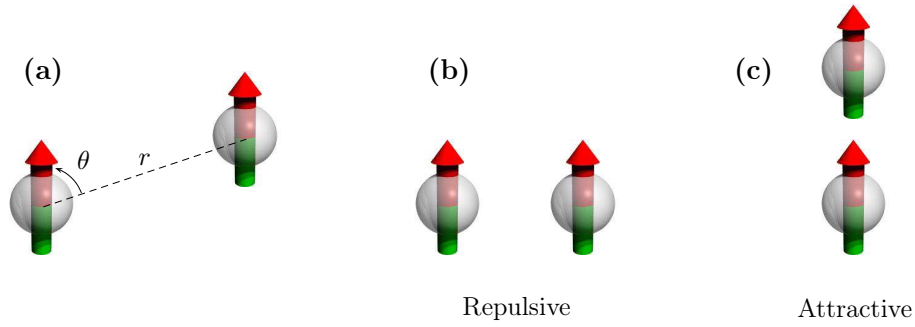
FIGURE 1. (a) Notations for the dipole-dipole interaction. (b) Dipoles placed side-to-side repel each other. (c) Dipoles in a 'head-to-tail' configuration attract each other.

The corresponding potential is

$$U_{dd}(\mathbf{r}) = \frac{C_{dd}}{4\pi} \frac{1 - 3\cos 2\theta}{r^3}, \tag{2}$$

where C_{dd} is the dipolar coupling constant ($C_{dd} = \mu_0 \mu^2$ for magnetic moments μ, $C_{dd} = d^2/\varepsilon_0$ for electric dipole moments d), and θ the angle between the direction joining the two dipoles and the dipole orientation (we assume here that all dipoles are aligned along the same direction z). The DDI is *anisotropic* (dipoles placed side-to-side repel each other, while dipoles in a head to tail configuration attract each other, see Fig.1) and *long range* (the $1/r^3$ dependence implies for example that the scattering cross-section is not isotropic in the low-energy limit).

To characterise the relative strength of the dipolar and contact interactions, it is convenient to introduce the dimensionless parameter

$$\varepsilon_{dd} \equiv \frac{C_{dd} m}{12\pi \hbar^2 a}. \tag{3}$$

The numerical factors in ε_{dd} are chosen such that a homogeneous BEC with $\varepsilon_{dd} > 1$ is unstable (see Sect.3.2.1 below). For the alkalis usually used in BEC experiments, the value of ε_{dd} is extremely small (for example, for ^{87}Rb, one has $\varepsilon_{dd} \simeq 0.007$), making the effects of the DDI negligible.

2.3. Ultra-cold systems with long-range interaction

There are several candidates to realize experimentally a dipolar quantum gas: molecules having a permanent electric dipole moment d, Rydberg atoms, which can have very large induced electric dipole moments, or ground state atoms having a large magnetic moment μ. In this section, we are going to briefly describe the main characteristics of those physical systems, and in the rest of this review, we will describe in detail the case of ultra-cold Chromium atoms, the only ones for which at present quantum degeneracy has been achieved.

2.3.1. Polar molecules

Heteronuclear molecules in their ground state have a large electric dipole moment, on the order of one Debye ($1\,\mathrm{D} \simeq 3.3 \times 10^{-30}\,\mathrm{C\cdot m}$). Assuming that the order of magnitude for the scattering length is similar to that of atoms used in BEC experiments (typically around $100a_0$, where a_0 is the Bohr radius), the corresponding value of $\varepsilon_{\mathrm{dd}}$ is on the order of 100, meaning that the properties of such a quantum gas would be dominated by the DDI.

To date, no quantum degenerate gas of polar molecules is available experimentally. Progress has been made recently in cooling of molecules (see ref. [25] for a review), but the densities and temperatures achieved so far are still orders of magnitude away from the quantum degenerate regime. A promising approach is to use Feshbach resonances in mixtures of ultra-cold fermions in order to create heteronuclear bosonic molecules. Those molecules created in a highly excited vibrational state must then be brought to the lowest vibrational state, e.g. by photoassociation.

2.3.2. Rydberg atoms

Another system in which large electric dipole moments can be achieved is given by Rydberg atoms. They are highly excited atoms, having large principal quantum number n and a dipole moment scaling like n^2. The mutual interaction depends on the atomic states involved. By means of an electric field, one can mix states with different electron orbital angular momentum, such that the atoms acquire a dipole moment and can interact to first order via dipole interaction. Due to the very large dipole moments, this interaction is very strong and is felt over very long distances, of the order of many tens of microns.

The state of the art in this field includes the observation of the blockade effect, which forbids more than one atom to be excited in a given region of space (defined by the distance where the interaction energy equals the linewidth of the excitation) and allows the production of an atomic ensemble with a single collective excitation. Moreover it includes the investigation of the resonant dipole-dipole interaction in an electric field (Förster resonance), collective behaviours and the real-time study of the dynamics of interacting pairs of Rydberg atoms, revealing the character of the long-range interactions. For more details, see e.g. [26] and references therein.

2.3.3. Paramagnetic atoms with large magnetic moments μ

Some atoms like Cr, Eu, Dy, have a large magnetic moment of several Bohr magnetons in their ground state. Only Cr has been Bose-condensed to date, and therefore the only quantum gas to display measurable dipolar effects is the Chromium BEC obtained in Stuttgart in 2004 [27]. Chromium has a magnetic dipole moment of $6\mu_B$, and a scattering length of about $100a_0$ (a_0 is the Bohr radius). This gives $\varepsilon_{\mathrm{dd}} \simeq 0.16$, which allows to observe a perturbative effect of the dipolar interaction.

3. BEC OF CHROMIUM

In this section, we give a very brief overview of the experimental sequence used to obtain a ^{52}Cr BEC. More details can be found for example in [28].

The specific level structure of Chromium makes it possible (and necessary) to use novel laser cooling strategies to load atoms continuously into a magnetic trap [29]. After Doppler cooling in the magnetic trap, we get a cloud of 1.5×10^8 atoms at a temperature of a few hundreds of μK [30]. RF-induced evaporative cooling is then performed. However, dipolar relaxation from the low-field-seeking state $|^7S_3, m_S = +3\rangle$ towards lower m_S states prevents condensation [31].

The cloud (with 6×10^6 atoms at about 20 μK) is thus transferred into a crossed optical dipole trap (50 W at 1070 nm), and atoms are optically pumped to the high-field-seeking state $|^7S_3, m_S = -3\rangle$, which is the absolute ground state; with a magnetic field of a few Gauss, dipolar relaxation is thus energetically suppressed. Forced evaporative cooling in the dipole trap then yields a pure condensate with up to 10^5 atoms [32].

3.1. Feshbach resonances in Chromium

Besides its large magnetic moment, Cr has another asset: 14 Feshbach resonances have been observed [33] for atoms in the state $|^7S_3, m_S = -3\rangle$. Close to such a resonance, the scattering length varies with the applied magnetic field B as

$$a(B) = a_{\rm bg} \left(1 - \frac{\Delta}{B - B_0} \right). \tag{4}$$

Here, B_0 is the resonance position, Δ its width, and $a_{\rm bg}$ the background (non-resonant) scattering length. This yields the possibility of increasing $\varepsilon_{\rm dd}$ by making a approach zero. For this, one needs to control the magnetic field B with a precision much better than Δ. The broadest known Feshbach resonance of Cr lies at $B_0 = 589$ G, and has a width of $\Delta = 1.4$ G. The small value of $\Delta/B_0 \simeq 2.3 \times 10^{-3}$ implies that one needs a good control of the field to tune a accurately (typically, a relative control of the field at the $\sim 10^{-5}$ level is needed to control a at the $\sim a_0$ level).

3.2. Dipolar expansion

The most spectacular effect of the magnetic dipole-dipole interactions (MDDI) on the Cr BEC in an anisotropic harmonic trap appears in time of flight experiments. The aspect ratio of the cloud during expansion is modified by the MDDI and depends on the orientation of the atomic dipoles with respect to the trap axes. In this section, we first give a summary of the theoretical tools used to describe such experiments, and then describe our results.

3.2.1. GPE for dipolar gases

Pure contact interaction: a reminder. Weakly interacting BECs with pure contact interaction are well described by the Gross-Pitaevskii equation (GPE) for the order parameter $\psi(\mathbf{r},t)$

$$i\hbar\frac{\partial\psi}{\partial t} = -\frac{\hbar^2}{2m}\triangle\psi + \left(V_{\text{ext}} + g|\psi|^2\right)\psi. \tag{5}$$

The non-linear term proportional to g accounts for the effect of interactions within the mean-field approximation. Note also that in the time-independent case, the left-hand side of the above equation has to be replaced by $\mu\psi$, with μ the chemical potential. The normalisation of ψ chosen here is $\int|\psi|^2 = N$, where N is the total atom number.

A useful reformulation of the Gross-Pitaevskii equation is obtained by writing $\psi = \sqrt{n}\exp(iS)$, with n the atomic density and S the phase of the order parameter, related to the superfluid velocity field by $\mathbf{v} = (\hbar/m)\nabla S$. Substituting in (5) and separating real and imaginary parts, one gets the following set of hydrodynamic equations

$$\frac{\partial n}{\partial t} + \nabla\cdot(n\mathbf{v}) = 0, \tag{6}$$

the equation of continuity, and an Euler-like equation

$$m\frac{\partial\mathbf{v}}{\partial t} + \nabla\left(\frac{mv^2}{2} + gn + V_{\text{ext}} - \frac{\hbar^2}{2m}\frac{\triangle\sqrt{n}}{\sqrt{n}}\right) = 0. \tag{7}$$

For the case of a uniform condensate ($V_{\text{ext}} = 0$), one easily shows, by linearising the hydrodynamic equations around equilibrium, that the frequency ω and wavevector k of a harmonic perturbation are linked by the following dispersion relation, the Bogoliubov spectrum

$$\omega = k\sqrt{\frac{gn}{m} + \frac{\hbar^2 k^2}{4m^2}}. \tag{8}$$

Dipolar interaction. To include dipolar effects, one just needs (as long as the DDI strength is not too high) to add an extra term to the mean-field potential $g|\psi|^2$, namely

$$\Phi_{\text{dd}}(\mathbf{r},t) = \int|\psi(\mathbf{r}',t)|^2 U_{\text{dd}}(\mathbf{r}-\mathbf{r}')\,d\mathbf{r}'. \tag{9}$$

This extra term is thus *non-local* (due to the long-range character of the DDI) and makes it much more complicated to solve the GPE, even numerically (one faces now an integro-differential equation). For very large dipolar interaction (in the case, e.g., of dipolar molecules), this simple modification of the Gross Pitaevskii equation is not valid any more, as the separation of length scales on which it relies (namely, that the scattering length entering the contact interaction is determined by the intermolecular potential at relatively small distances, where the effects of the DDI are small compared to the van der Waals interaction) breaks down. In that case, the contact interaction depends on the strength of the dipolar coupling.
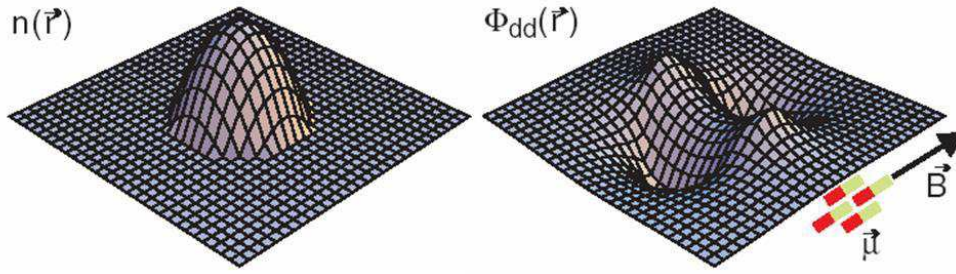
FIGURE 2. Density distribution for a non-dipolar BEC in an isotropic trap (left). The resulting dipolar potential Φ_{dd} has a saddle-like shape, which tends to elongate the condensate along the magnetization direction (right). Figure taken from [27].

As a simple application, one can calculate the modifications to the Bogoliubov spectrum induced by the DDI [34]. Using the fact that the Fourier transform of the DDI (2) takes the form

$$\widetilde{U_{dd}}(\mathbf{k}) = C_{dd}(\cos^2 \alpha - 1/3), \tag{10}$$

where α is the angle between $\mathbf{k}$ and the direction of the dipoles, and following the same method as in the previous paragraph, one easily shows that the excitation spectrum is now given by

$$\omega = k \sqrt{\frac{n}{m}\left[g + \frac{C_{dd}}{3}(3\cos^2 \alpha - 1)\right] + \frac{\hbar^2 k^2}{4m^2}}, \tag{11}$$

and that, with the definition (3) for ε_{dd}, this implies that a dipolar uniform condensate is unstable for $\varepsilon_{dd} > 1$.

3.2.2. *Thomas-Fermi solutions and scaling Ansatz for the expansion*

Static Thomas-Fermi solutions. For pure contact repulsive interaction, when the atom number is increasing, the condensate size increases and the zero-point kinetic energy becomes smaller and smaller. The Thomas-Fermi approximation consists in neglecting the kinetic energy term in the time-independent GPE; this gives then a simple algebraic equation, showing that the density distribution has the shape of an inverted parabola.

It is remarkable that this property remains valid if dipolar interaction is included. This is due to the fact that the dipolar mean-field potential $\Phi_{dd}(\mathbf{r})$ for a parabolic density distribution $n(\mathbf{r}) = |\psi(\mathbf{r})|^2$ is quadratic in the coordinates (having a saddle shape because of the anisotropy, Fig.2) [35].

For the case of a spherically symmetric trap (and thus also a spherically symmetric density distribution for pure contact interaction), one can easily show that, to first order in ε_{dd}, the effect of the MDDI is to elongate the condensate along the direction of

magnetization: it is energetically favourable to accommodate new particles close to the magnetization axis, where $\Phi_{dd}(\mathbf{r})$ is minimum (see Fig.2), thus causing an elongation of the condensate. It is possible to show that this behaviour is valid for anisotropic traps and for higher values of ε_{dd}. Note however that for a non-spherical density distribution, calculating the coefficients of the quadratic terms in Φ_{dd} is possible but beyond the scope of this paper. See [35] for details.

Expansion: scaling Ansatz. For a pure contact interaction, and in the Thomas-Fermi approximation, namely $Na/a_{ho} \gg 1$ with $a_{ho} = \sqrt{\hbar/(m\bar{\omega})}$, there exists a very useful solution of the GPE [36]. It shows that the inverted parabola shape of the condensate is maintained upon expansion (after release from the trap), with a mere *rescaling* of its radii. The scaling parameters $b_i(t)$ $(i = x, y, z)$ giving the radii $R_i(t) = R_i(0)b_i(t)$ are solutions of the ordinary differential equations

$$\ddot{b}_i = \frac{\omega_i^2(0)}{b_i \prod\limits_{j \in \{x,y,z\}} b_j} \qquad (i \in \{x,y,z\}). \tag{12}$$

Like for the static case, this can be extended to the case of dipolar interactions, since Φ_{dd} keeps a parabolic shape. The corresponding equations now read

$$\ddot{b}_i = \frac{\omega_i^2(0)}{b_i \prod\limits_{j \in \{x,y,z\}} b_j} + f(\{b_j\}; \{\omega_j\}; \varepsilon_{dd}) \qquad (i \in \{x,y,z\}), \tag{13}$$

where f is a function of the scaling radii, trap frequencies, and dipolar parameter ε_{dd}. It turns out that the elongation of the condensate along the magnetization direction remains valid during expansion. The reader is again referred to [35] for further details.

3.3. Experiments

3.3.1. MDDI as a small perturbation

The first demonstration of an effect of the MDDI in a quantum gas came soon after the first realization of a Cr BEC, by measuring the aspect ratio of the BEC during time-of-flight for two different orientations of the dipoles with respect to the trap axes. The small value $\varepsilon_{dd} \simeq 0.16$ implied that the effect was only a small perturbation on top of the expansion driven by the contact interaction (see Fig. 3).

#### 3.3.2. Use of the Feshbach resonance: strong dipolar regime

To go beyond this perturbative effect, we used the 589 G Feshbach resonance of Cr, in order to reduce a, and thus enhance ε_{dd}. We provide this field using the offset coils of the magnetic trap, with a current of about 400 amperes, actively stabilised at a level of
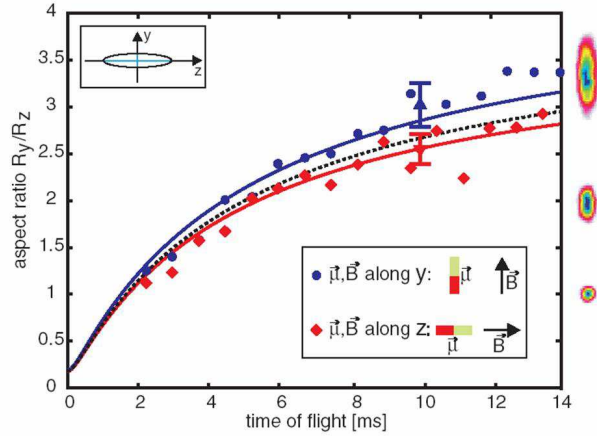
FIGURE 3. MDDI as a small perturbation in the expansion of a condensate. The aspect ratio is measured during expansion for two different orientations of the dipoles with respect to the trap axes. Figure taken from [27].

4×10^{-5} in relative value (peak to peak). The field is switched on during the evaporation sequence in the ODT, at a stage when the density is not too high, in order not to lose too many atoms by inelastic losses when crossing the Feshbach resonances. The rest of the experiment is performed in high field. After a BEC is obtained, we ramp the field close to the resonance in 10 ms, hold the field there for 2 ms, and take an absorption picture (still in high field) after 5 ms of time of flight.
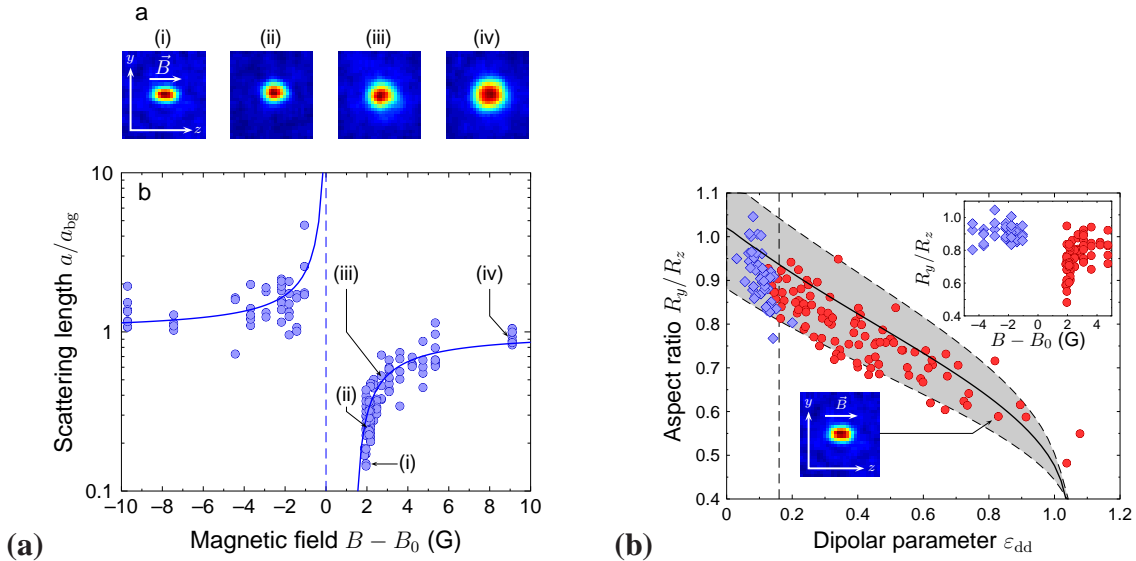
FIGURE 4. (a) Measured scattering length $a(B)$ across the Feshbach resonance at $B_0 = 589$ G. The condensate images (i)-(iv) in the top of the figure clearly show a modification of the size (due to the reduction of a) and of the aspect ratio (due to enhanced dipolar effects) of the condensate. (b) Aspect ratio of the BEC after 5 ms of expansion, as a function of the measured dipolar parameter ε_{dd}. The solid line corresponds to the prediction of hydrodynamic equations in the Thomas-Fermi limit. Figure taken from [18].
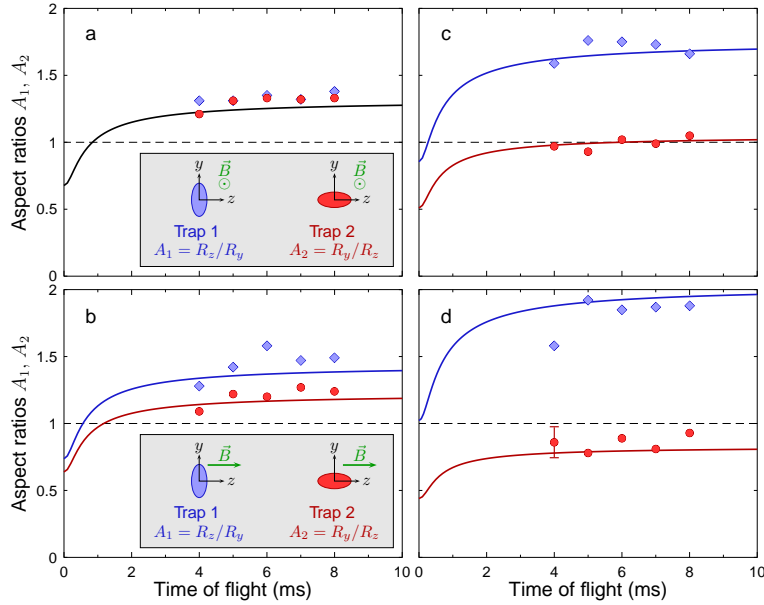
FIGURE 5. Aspect ratio of the BEC vs time of flight. (a) $\varepsilon_{dd} = 0.16$, magnetic field along x, the aspect ratio is the same for the two trap configurations as expected. (b) $\varepsilon_{dd} = 0.16$, magnetic field along z, one basically recovers the results of Fig.3. (c) $\varepsilon_{dd} = 0.5$. d: $\varepsilon_{dd} = 0.75$, the inversion of ellipticity of the cloud is inhibited by the MDDI. Figure taken from [18].

From the density distribution, we measure the Thomas-Fermi radii of the BEC, and we infer the value of the scattering length (taking into account explicitly the MDDI interaction by solving Eqs. (13)). The measured a is shown on Fig. 4 (a). One can see clearly a five-fold reduction of a above resonance, corresponding to a maximal value of $\varepsilon_{dd} \simeq 0.8$. On the sample absorption images of Fig. 4 (a), one clearly sees, when B approaches $B_0 + \Delta$, a strong reduction of the BEC size, due to the reduction of a, and thus of the mean field energy released upon expansion[1]. But one also clearly observes an elongation of the BEC along the magnetic field direction z. This change in the cloud aspect ratio would not happen for a pure contact interaction and is a direct signature of the MDDI. Fig. 4 (b) shows the aspect ratio of the cloud as a function of ε_{dd}, together with the theoretical prediction from (13).

As an application of the tunability of ε_{dd}, we measured the aspect ratio of the BEC during expansion for two different orientations of the dipoles with respect to the trap axes. The effect of MDDI is now way beyond the perturbative regime (Fig.5). For large enough ε_{dd}, one clearly sees that the usual inversion of ellipticity of the BEC during expansion is inhibited by the MDDI.

Such tuning of the scattering length by means of a Feshbach resonance is a first step in the study of the properties of purely dipolar quantum gases ($\varepsilon_{dd} \gg 1$). Future directions of study include e.g. the dependence of the stability of a dipolar BEC on the trap geometry, or the behaviour of dipolar quantum gases in optical lattices.

---

[1] For a pure contact interaction, the TF radius after expansion scales as $(Na)^{1/5}$.

4. ULTRA-COLD ATOMS IN OPTICAL LATTICES

The possibility of trapping and manipulating cold atomic gases with the degree of freedom and precision described above allows to investigate a huge range of different physical systems, where one has control on the system geometry, the interatomic interactions and the statistics of the atoms. One of the most fruitful fields of research both from the experimental and the theoretical point of view in the last years has been the study of ultra-cold atomic samples in optical lattices.

Optical lattices are non dissipative periodic potential energy surfaces for the atoms created by the intersection of laser fields. The investigation of cold atoms in periodic potentials allows to reproduce problems traditional of condensed matter and solid state physics in a new setting, where a high degree of control is possible and where the Hamiltonian which governs the system is in general very close to some idealised one.

One of the greatest achievements of the last years was the experimental observation of the superfluid to Mott insulator transition (for details, see Sect.4.1) [12, 37, 38]. In presence of long-range interactions, additional quantum phases are predicted [39, 40, 41, 42], like the supersolid phase, presenting the coexistence of superfluidity and periodic spatial modulation, whose existence has not yet been unambiguously proven experimentally [43]. The search for this and other quantum phases makes cold atoms with long range interactions particularly appealing.

As we will explain in the following, there are striking effects of long range interactions to be expected for ultra-cold atoms in optical lattices. Even if their existence strictly depends on the long-range character of the interactions, their observability might require a relative strength of the dipole-dipole interaction not too small compared to the zero-range one. For this reason the recent achievements with Chromium atoms presented in Sect.3.3.2 are particularly important for the possible experimental realization of the systems that we are going to discuss in the following.

First, we will introduce the main theory for ultra-cold atoms in optical lattices in the extensively studied and experimentally already realized case of point-like interaction. This will provide the background for the topic of our interest, namely the case of long-range interactions.

4.1. Point-like interaction: superfluid to Mott insulator transition

As previously explained, in the most common cases, ultra-cold atoms interact via s-wave scattering, which can be in a very good approximation considered a point-like interaction. Then, the Hamiltonian of the system in second quantisation reads

$$
\begin{aligned}
H \;=\; & \int \hat{\psi}^{\dagger}(\mathbf{r}) \left(\frac{p^2}{2m} + V_{\text{ext}}(\mathbf{r}) \right) \hat{\psi}(\mathbf{r})\, d\mathbf{r} + \frac{g}{2} \int \hat{\psi}^{\dagger}(\mathbf{r}) \hat{\psi}^{\dagger}(\mathbf{r}) \hat{\psi}(\mathbf{r}) \hat{\psi}(\mathbf{r})\, d\mathbf{r} \\
& - \mu \int \hat{\psi}^{\dagger}(\mathbf{r}) \hat{\psi}(\mathbf{r})\, d\mathbf{r},
\end{aligned}
\tag{14}
$$

where $\hat{\psi}(\mathbf{r})$ is the field operator, $V_{\text{ext}}(\mathbf{r})$ the trapping potential, g the interaction strength, linked to the s-wave scattering length through $g = 4\pi\hbar^2 a/m$, and μ the chemical potential, which fixes the total number of particles.

In the presence of an optical lattice, the trapping potential is periodic $V_{\text{ext}}(\mathbf{r}) = \sum_n V_n^{opt} sin^2(\pi x_n/d_n)$, where the index n runs over the dimensions of the lattice, and where d_n is the lattice constant in the n-th direction. For lattices created by counterpropagating laser beams of wavelength λ, the lattice spacing is $d = \lambda/2$. The intensity of the lattice potential V_n^{opt} depends on the intensity of the laser light.

As it is well known [44], the spectrum of a single particle in a periodic potential is characterised by bands of allowed energies and energy gaps. For deep enough periodic potentials, the so-called tight binding regime is reached, where the first band takes the form $E(q) = -2J \sum_n cos(q_n d)$, being q_n the quasi-momenta in the different lattice directions and J is the tunneling parameter between neighbouring wells.

Provided the lattice is deep enough and for low enough interactions and temperature, the physics of the system can be well approximated by the one taking place in the first energy band. The counterpart of the energy eigenstates delocalised over the whole lattice (Bloch states) are the wavefunctions localised at the bottom of each lattice site (Wannier functions). In the tight binding regime is often convenient to use the Wannier description.

In the single band approximation, the field operator can be replaced by its single-mode expansion

$$\hat{\psi}(\mathbf{r}) = \sum_i w_i(\mathbf{r})\hat{a}_i, \tag{15}$$

with $\hat{a}_i$ being the annihilation operator for one boson in the Wannier function $w_i(\mathbf{r})$ localised at the bottom of lattice site i. Plugging this expression in the second quantised Hamiltonian, one gets

$$
\begin{aligned}
H &= \sum_{i,j} \int w_i^*(\mathbf{r}) \left(\frac{p^2}{2m} + V_{\text{ext}}(\mathbf{r}) \right) w_j(\mathbf{r}) \, d\mathbf{r} \; \hat{a}_i^\dagger \hat{a}_j + \\
&\quad + \frac{g}{2} \sum_{i,j,l,m} \int w_i^*(\mathbf{r}) w_j^*(\mathbf{r}) w_l(\mathbf{r}) w_m(\mathbf{r}) \, d\mathbf{r} \; \hat{a}_i^\dagger \hat{a}_j^\dagger \hat{a}_l \hat{a}_m - \mu \sum_i \hat{a}_i^\dagger \hat{a}_i,
\end{aligned}
\tag{16}
$$

where in the chemical potential term we have exploited the orthonormality of the Wannier functions.

For deep enough lattices, where the overlap beyond nearest neighbours can be neglected, and defining

$$J = -\int w_i^*(\mathbf{r}) \left(\frac{p^2}{2m} + V_{\text{ext}}(\mathbf{r}) \right) w_{i+1}(\mathbf{r}) \, d\mathbf{r}, \tag{17}$$

$$U = g \int |w_i(\mathbf{r})|^4 \, d\mathbf{r}, \tag{18}$$

one gets, a part from constant terms,

$$H = -J \sum_{\langle ij \rangle} \hat{a}_i^\dagger \hat{a}_j + \sum_i \left[\frac{U}{2} n_i(n_i - 1) - \mu n_i \right], \tag{19}$$

with $n_i = \hat{a}_i^\dagger \hat{a}_i$ being the density operator at site i.

This is the famous Bose-Hubbard Hamiltonian, extensively studied in condensed matter physics. In optical lattices the Hamiltonian parameters can be accurately controlled by changing the strength of the optical lattice: ramping it up increases interactions due to a stronger localisation of the wavefunctions at the bottom of the lattice wells, and at the same time exponentially decreases tunneling.

When tunneling is suppressed compared to interactions, this Hamiltonian presents a quantum phase transition between a superfluid phase, characterised by large number fluctuations at each lattice site, and a Mott insulating phase where each lattice well is occupied by precisely an integer number of atoms without any number fluctuations. The nature of this phase transition and the qualitative phase diagram can be inferred based on very simple arguments.

At zero tunneling $J = 0$ and commensurate filling (exactly an integer number n of atoms per well), the interaction energy is minimised by populating each lattice well by exactly n atoms. Energy considerations can tell which is the range of chemical potential μ at which the filling factor n is the most energetically convenient:

$$\begin{aligned}
E(n) &= \frac{U}{2} n(n-1) - \mu n, \\
E(n) &< E(n+1) \quad \text{and} \quad E(n) < E(n-1) \Rightarrow \\
(n-1)&U < \mu < nU.
\end{aligned} \tag{20}$$

This state with precisely integer occupation at the lattice sites is called Mott insulating state. Since a particle-hole excitation at $J = 0$ costs an energy $\Delta E = U$ equal to the interaction energy, the Mott state is the lowest energy state at commensurate filling (see Fig.6). For a tunneling J different from zero the energy cost to create an excitation decreases thanks to the kinetic energy favouring particle hopping. However, for large interactions and small tunneling, the gain in kinetic energy ($\sim J$) is not yet sufficient to overcome the cost in interaction energy ($\sim U$), which leads to the existence of Mott insulating states also at finite tunneling. For large enough tunneling, instead, particle hopping becomes energetically favourable and the system becomes superfluid. The regions in the J vs. μ phase diagram where the Mott insulating state is the ground state are called *Mott lobes*. For non commensurate filling, there are extra atoms free to hop to site to site at no energy cost, so that the phase of the system is always superfluid. The superfluid phase at non commensurate densities survives down to $J = 0$ for $\mu/U = [\rho]$ where the symbol $[\rho]$ indicates the integer part of the density.

Due to the finite energy cost required to add or remove one particle, the Mott phase is gapped and incompressible, while in the superfluid regions the gap vanishes and the system is compressible.

In Eq.(20) we have identified the boundaries of the Mott lobes at $J = 0$. In order to find the shape of the lobes at finite J more sophisticated calculations are required. In
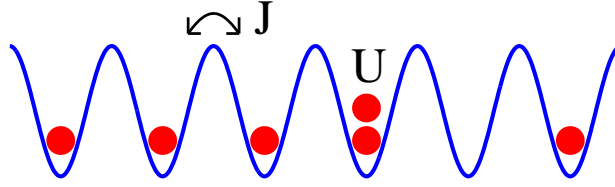
FIGURE 6. Sketch of a particle-hole excitation in the $n = 1$ Mott phase. The energy cost for having two particles in the same site is U and the energy gained by hopping is $\sim J$. Their interplay determines whether the ground state is insulating or superfluid.

particular there is no exact analytical method which allows to calculate them. A part from the mean-field approximation [37, 45, 46], which is discussed later, high order perturbative strong coupling expansions can be performed [47]. Exact numerical results can be obtained using Quantum Monte Carlo techniques [48].

In the next sections, we introduce the mean-field approximation and the perturbative method that we use to calculate the lobes. It works only qualitatively in one dimension and work better and better in larger dimensions. This will provide further insight on the conditions required for the insulating lobes to exist and proves very useful to understand the analogies and differences in the case of long-range interactions.

In the non uniform geometries available in the experiments, where a harmonic potential is superimposed to the optical lattice, the trapping potential is taken into account in the Bose-Hubbard Hamiltonian through a site-dependent chemical potential $\mu_i = \mu - V_i$, being V_i the harmonic potential at site i. The system is characterised by alternating shells of Mott and superfluid phases [38, 49, 50]. In this paper we will concentrate on the uniform system and not discuss the trapped system in more detail.

4.1.1. Mean-field decoupling and Gutzwiller Ansatz

Starting from the Bose-Hubbard Hamiltonian (19), one can perform the so-called mean-field decoupling [37, 45, 46]. We define the order parameter $\langle a \rangle = \varphi$ and proceed with the following substitution

$$a = \tilde{a} + \varphi, \ a^\dagger = \tilde{a}^\dagger + \varphi^*, \tag{21}$$

obtaining for the hopping term

$$-J \sum_{\langle ij \rangle} \left[\varphi_i^* \left(\hat{a}_j - \frac{\varphi_j}{2} \right) + \varphi_j \left(\hat{a}_i^\dagger - \frac{\varphi_i^*}{2} \right) + \tilde{a}_i^\dagger \tilde{a}_j \right]. \tag{22}$$

Based on this result, the full Hamiltonian can be rewritten with no approximations as

$$H = -J \sum_{\langle ij \rangle} \left[\varphi_i^* \left(\hat{a}_j - \frac{\varphi_j}{2} \right) + \varphi_i \left(\hat{a}_i^\dagger - \frac{\varphi_i^*}{2} \right) + \tilde{a}_i^\dagger \tilde{a}_j \right] + \sum_i \left[\frac{U}{2} n_i (n_i - 1) - \mu n_i \right], \tag{23}$$

where the term $\tilde{a}_i^\dagger \tilde{a}_j$ is supposed to be small.

The full Hamiltonian in the mean-field approximation is just given by the sum of the mean-field Hamiltonians on different sites $H^{MF} = \sum_i H_i^{MF}$, where

$$H_i^{MF} = -J\left[\bar{\varphi}_i^*\left(\hat{a}_i - \frac{\varphi_i}{2}\right) + \bar{\varphi}_i\left(\hat{a}_i^\dagger - \frac{\varphi_i^*}{2}\right)\right] + \frac{U}{2}n_i(n_i - 1) - \mu n_i \qquad (24)$$

and $\bar{\varphi}_i = \sum_{\langle j \rangle_i} \varphi_j$ takes the neighbouring wells into account at the mean-field level.

In the homogeneous system, all order parameters $\varphi_i = \varphi$ are equal. For each set of parameters U, J, μ, one can find the value of φ which minimises the ground state eingevalue (at $T = 0$). A vanishing order parameter is the indication of a Mott insulating phase, while an order parameter different from zero, which can be only produced by number fluctuations at the lattice sites, is the signature of a superfluid state. The mean-field solution found in this way is completely equivalent to the one provided by the famous Gutzwiller Ansatz. This corresponds in writing the state of the system as a product over the different lattice sites of single-site wavefunctions

$$|\Phi(t)\rangle = \prod_i \sum_n f_n^{(i)}(t)|i,n\rangle, \qquad (25)$$

where i is the site label and n indicates the number state. The coefficients $f_n^{(i)}$ are called Gutzwiller coefficients.

The solution obtained by the Gutzwiller Ansatz is intrinsically mean-field. On the other hand it allows to extract many important information and study the dynamics of the system. In fact, through a time dependent variational approach based on the Lagrangian

$$\mathcal{L} = \frac{\langle\dot{\Phi}|\Phi\rangle - \langle\Phi|\dot{\Phi}\rangle}{2i} - \langle\Phi|H|\Phi\rangle, \qquad (26)$$

one obtains the dynamical equations for the Gutzwiller coefficients

$$i\frac{d f_n^{(i)}}{dt} = -J\left[\bar{\varphi}_i\sqrt{n_i}f_{n-1}^{(i)} + \bar{\varphi}_i^*\sqrt{n_i+1}f_{n+1}^{(i)}\right] + \left[\frac{U}{2}n_i(n_i-1) - \mu n_i\right]f_n^{(i)}. \qquad (27)$$

By solving those equations in imaginary ($\tau = it$) time, one accesses the stationary states of the system, while in real time the dynamics of the system can be investigated also in the case of time-dependent Hamiltonian parameters [51].

4.1.2. Mean-field perturbative approach

The mean-field perturbative approach allows to find the boundaries of the lobes in an analytical way. The main approximation underlying this method is the mean-field

approximation described in the previous section. For the purposes of this section, we separate the Hamiltonian in two parts

$$H_0 = \sum_i \left[\frac{U}{2} n_i (n_i - 1) - \mu n_i \right], \tag{28}$$

$$H_J = -J \sum_i \left[\bar{\varphi}_i^* \left(\hat{a}_i - \frac{\varphi_i}{2} \right) + \bar{\varphi}_i \left(\hat{a}_i^\dagger - \frac{\varphi_i^*}{2} \right) \right], \tag{29}$$

where we remind that $\varphi_i = \langle \hat{a}_i \rangle$ is the order parameter and $\bar{\varphi}_i = \sum_{\langle j \rangle_i} \varphi_j$ is the sum of the order parameters at sites neighbouring to a given site i.

The term H_J replaces the non-local tunneling term present in the full Hamiltonian. Assuming that the order parameters φ_i are small, we rewrite H_J at first order in the order parameter as

$$H_J \approx -J \sum_i \left[\bar{\varphi}_i^* \hat{a}_i + \bar{\varphi}_i \hat{a}_i^\dagger \right]. \tag{30}$$

We use this approximate expression in the calculation of the partition function

$$\mathscr{Z} \approx Tr \left[e^{-\beta H_0} \right] - \int_0^\beta Tr \left[e^{-(\beta - \tau)H_0} H_J e^{-\tau H_0} \right] d\tau + \mathscr{O}(\varphi^2) = Tr \left[e^{-\beta H_0} \right], \tag{31}$$

where we have used that H_J is first order in the creation and destruction operators and neglected second order terms. In the limit $\beta \to \infty$, corresponding to zero temperature, the partition function becomes

$$\mathscr{Z} \equiv \mathscr{Z}_0 = e^{-\beta E_0}, \tag{32}$$

being E_0 the energy of the ground state. In the calculation of the order parameter instead, the first order term in the creation and destruction operators also contributes, in the form

$$
\begin{aligned}
\varphi_i &\approx -e^{\beta E_0} \int_0^\beta Tr \left[\hat{a}_i e^{-(\beta - \tau)H_0} H_J e^{-\tau H_0} \right] d\tau = \\
&= J \bar{\varphi}_i e^{\beta E_0} \int_0^\beta Tr \left[\hat{a}_i e^{-(\beta - \tau)H_0} \hat{a}_i^\dagger e^{-\tau H_0} \right] d\tau, \tag{33}
\end{aligned}
$$

where we have used the definition of H_J at first order in the order parameter, the fact that the expectation value of two destruction operators over eigenstates of H_0 vanishes, and the fact that non local averages vanish in the mean-field approximation. For the trace, we need to take into account all the matrix elements of the kind $\langle \Phi | \hat{a}_i e^{-(\beta - \tau)H_0} \hat{a}_i^\dagger e^{-\tau H_0} | \Phi \rangle$. The two creation and annihilation operators in this expectation value produce

$$\left(n_i^{|\Phi\rangle} + 1 \right) exp\left[-\beta H_0^{|\Phi+1,i\rangle} \right] exp\left[-\tau \left(H_0^{|\Phi\rangle} - H_0^{|\Phi+1,i\rangle} \right) \right], \tag{34}$$

where $|\Phi+1,i\rangle$ is the notation we use for the state which is obtained from state $|\Phi\rangle$ by creating one more particle at site i and $n_i^{|\Phi\rangle}$ is the number of atoms at site i in state $|\Phi\rangle$.

The integration over τ in the range $\tau \in [0,\beta]$, in the limit $\beta \to \infty$ and the multiplication by $e^{\beta E_0}$ give

$$\left(n_i^{|\Phi\rangle} + 1 \right) \left[\frac{exp\left[\beta \left(E_0 - H_0^{|\Phi+1,i\rangle} \right) \right]}{H_0^{|\Phi\rangle} - H_0^{|\Phi+1,i\rangle}} - \frac{exp\left[\beta \left(E_0 - H_0^{|\Phi\rangle} \right) \right]}{H_0^{|\Phi\rangle} - H_0^{|\Phi+1,i\rangle}} \right]. \tag{35}$$

Since by definition of ground state $E_0 - H_0^{|\Phi\rangle} \leq 0$ for all states $|\Phi\rangle$, this result converges to a non zero result if and only if either

1) $|\Phi\rangle$ is the ground state or $\qquad\qquad\qquad\qquad\qquad$ (36)

2) $|\Phi+1,i\rangle$ is the ground state, i.e. $|\Phi\rangle$ is the state
    obtained by removing one particle from the ground state at site i.

Namely, only two terms contribute to the trace (33): the one arising from the ground state $\langle GS|\hat{a}_i e^{-(\beta-\tau)H_0}\hat{a}_i^\dagger e^{-\tau H_0}|GS\rangle$ and the one arising from the states which are obtained from the ground state by removing one particle $\langle GS-1,i|\hat{a}_i e^{-(\beta-\tau)H_0}\hat{a}_i^\dagger e^{-\tau H_0}|GS-1,i\rangle$.

Hence, for a Mott state with integer well occupation equal to n_i, the order parameter reads

$$\varphi_i = \bar{\varphi}_i J \left[\frac{n_i+1}{Un_i-\mu} + \frac{n_i}{\mu - U(n_i-1)} \right]. \tag{37}$$

In a uniform system in the presence of point-like interaction φ_i is uniform and the solution can be found analytically. Given that $\bar{\varphi} = z\varphi$, being z the number of nearest neighbours, the order parameter $\varphi = 0$ unless

$$1 - zJ \left[\frac{n+1}{Un-\mu} + \frac{n}{\mu-U(n-1)} \right] = 0, \ i.e. \ zJ = \frac{(Un-\mu)(\mu-U(n-1))}{\mu+U}. \tag{38}$$

This equation has solutions (for $zJ > 0$) only for chemical potentials in the range $n-1 < \mu/U < n$, as already anticipated in Eq.(20).

Expression (38) of μ as a function of J defines the boundary of the Mott lobe at filling factor n. Outside of the lobes the order parameter becomes different from zero, indicating the arising of the superfluid phase. Then, this treatment, valid at 1st order in φ, is not valid anymore to predict the value of the order parameter. However, in the framework of the mean-field approximation, the expression for the lobes boundary is exact. Moreover,

most important, the prediction about the existence of the lobes, i.e. the lobes boundaries at $J = 0$, are exact also beyond the mean-field approximation and confirmed by exact numerical methods.

For the comparison that we will make later with the case of long-range interaction it is useful to state the condition for the existence of the lobes as follows: given an insulating state (classical distribution of atoms in the lattice), this is stable in a given range of chemical potential at $J = 0$ if the energy increases by adding or removing a particle at any site of the lattice, as depicted in Fig.7.
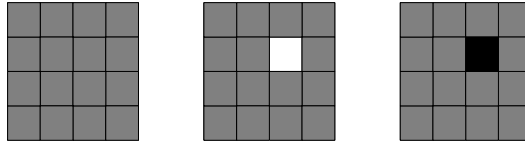
FIGURE 7.   Sketch of a Mott insulating $n = 1$ phase with energy $E(n = 1)$ (left); configuration where 1 atom has been removed, with energy $E(n = 1, -1, i) = E(n = 1) + \mu$ (center); configuration where 1 atom has been added, with energy $E(n = 1, +1, i) = E(n = 1) - \mu + U$ (right). For $0 < \mu < U$, the Mott $n = 1$ phase is the ground state.
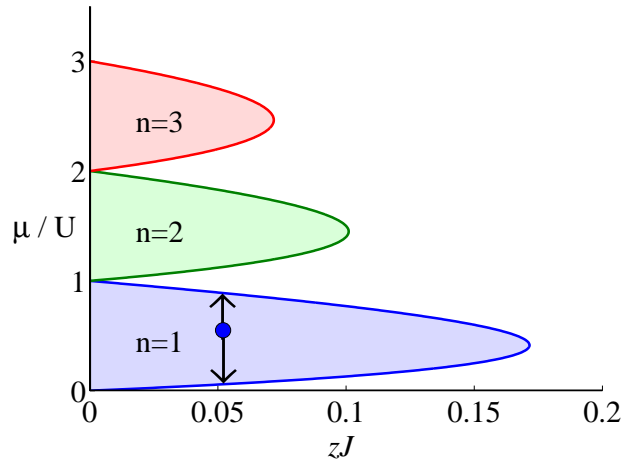
4.1.3. Phase diagram

Starting from Eq.(38) we can built the phase diagram of the system in the mean-field approximation, as shown in Fig.8. Inside the lobes the system in in the Mott insulating phase. For a given tunneling parameter J and chemical potential μ the energy for adding or removing a particle from the system is respectively given by the distance to the upper and lower lobe boundaries (at constant J). The sum of those energies (width of the lobe at constant J) gives instead the energy for a particle-hole excitation conserving the total number of atoms.

At the lobe boundary a quantum phase transition to the superfluid phase takes place. The tip of the lobe is a special point, because there the phase transition happens at commensurate filling factor n and is purely due to the effect of increased tunneling. At constant non commensurate density the system is always superfluid. For $J \to 0$, the lines of constant density accumulate between the Mott lobes, at integer values of $\mu/U = n$ where the energies for having n or $n + 1$ particle per site are equal.

5. LONG-RANGE INTERACTIONS IN OPTICAL LATTICES

We now consider dipolar atoms in a 2D optical lattice. In present experiments, usually 2D geometries are created as a series of pancake traps by means of a very strong 1D optical lattice in the perpendicular direction, which provides strong confinement and completely suppresses tunneling in one direction. In the presence of long-range interaction, in order to consider each layer to be isolated, one should not only suppress tunneling but also reduce the interaction between the different layers. For our purposes, where each layer contains a 2D lattice, one should make the distance between the

FIGURE 8. Phase diagram in the mean-field approximation. The boundaries of the Mott lobes are given by Eq.(38). The upwards and downwards arrows describe respectively the energy of a particle and hole excitation, as described in the text. Their sum is the energy of a particle-hole excitation.

different layers larger than the lattice spacing in the 2D plane. This can be achieved by creating a 2D lattice with two pairs of counterpropagating laser beams and the extra 1D lattice in the perpendicular direction by two laser beams intersecting at a given angle θ, as depicted in Fig.9, in order to increase the lattice spacing in the third direction to $d_{1D} = (\lambda/2)/sin(\theta/2)$.
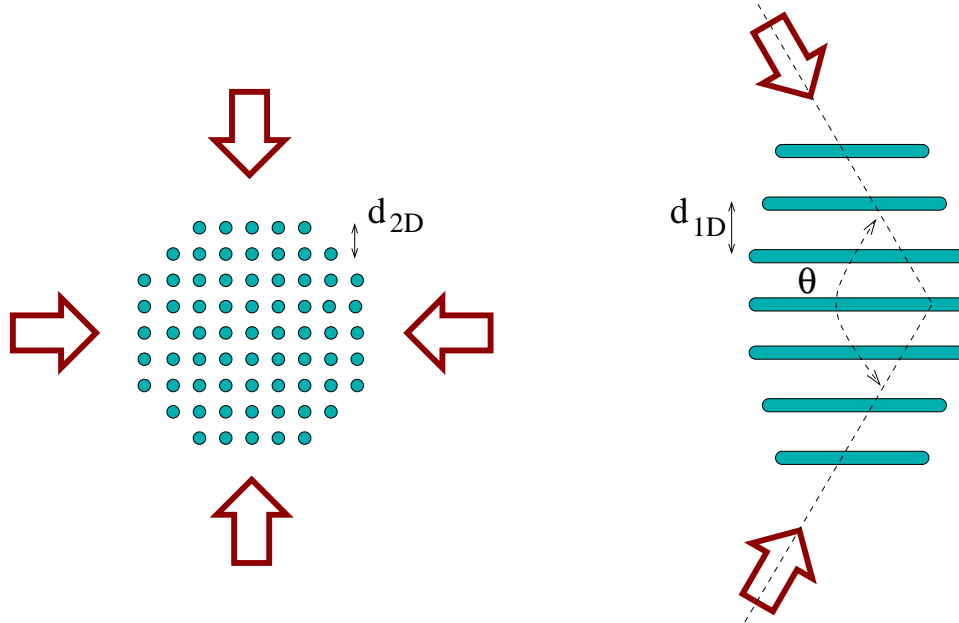
FIGURE 9. Two-dimensional lattice potential obtained by the intersection of four counter-propagating laser beams. For a wavelength λ the lattice spacing is given by $d_{2D} = \lambda/2$ (left); extra one-dimensional lattice in the perpendicular direction, obtained by the intersection of two laser beams at and angle θ; the lattice spacing is given by $d_{1D} = (\lambda/2)/sin(\theta/2)$ (right).

We consider an orientation of the dipoles perpendicular to the planes of the 2D lattice. This implies a repulsive interaction in the plane and an attractive interaction between different layers. The effect of this intra-layer attraction has been studied in [52]. We expect that the attractive character of the interaction in the perpendicular direction might even help in reproducing in the different layers the distribution of atoms that we find to exist in the single plane. However, to draw exact conclusions one should devote to this topic further studies. In the following we are going to restrict ourselves to the study of a single lattice plane.

5.1. Extended Bose-Hubbard model

In the presence of long-range interaction, an extra term has to be added to the Hamiltonian of the system, which in second quantisation reads

$$
\begin{aligned}
H \;=\; & \int \hat{\psi}^\dagger(\mathbf{r}) \left(\frac{p^2}{2m} + V_{\text{ext}}(\mathbf{r}) \right) \hat{\psi}(\mathbf{r})\, d\mathbf{r} + \frac{g}{2} \int \hat{\psi}^\dagger(\mathbf{r}) \hat{\psi}^\dagger(\mathbf{r}) \hat{\psi}(\mathbf{r}) \hat{\psi}(\mathbf{r})\, d\mathbf{r} + \\
& + \int\int \hat{\psi}^\dagger(\mathbf{r}') \hat{\psi}^\dagger(\mathbf{r}') U_{\text{dd}}(\mathbf{r}-\mathbf{r}') \hat{\psi}(\mathbf{r}) \hat{\psi}(\mathbf{r})\, d\mathbf{r}\, d\mathbf{r}' - \mu \int \hat{\psi}^\dagger(\mathbf{r}) \hat{\psi}(\mathbf{r}) d\mathbf{r}, \quad (39)
\end{aligned}
$$

where $U_{\text{dd}}(\mathbf{r})$ is the dipole-dipole potential defined in Eq.(2).

In the single band approximation, the generalised Bose-Hubbard Hamiltonian in the presence of long-range interaction becomes

$$
H \;=\; -J \sum_{\langle ij \rangle} \hat{a}_i^\dagger \hat{a}_j + \sum_i \left[\frac{U}{2} n_i(n_i - 1) - \mu n_i \right] + \sum_{\vec{\ell}} \sum_{\langle ij \rangle_{\vec{\ell}}} \frac{U_{\vec{\ell}}}{2}\, n_i n_j, \quad (40)
$$

where $\vec{\ell}$ is the distance connecting the two optical lattice sites i and j. The sum over the distance $\vec{\ell}$ is cut-off at a certain nearest neighbour. In our calculations we usually considered up to the $4th$ nearest neighbour, as shown in Fig.10. Longer interaction ranges have a crucial effect on the regions of the phase diagram describing low density of particles and holes [53], but we are not going to discuss this here.
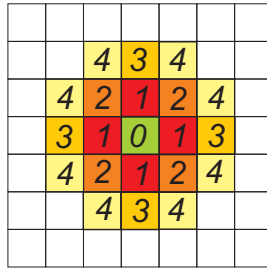
FIGURE 10. Representation of the first four nearest neighbours in a 2D optical lattice.

The on-site interaction parameter U is now given by two contributions: one is, as before, arising from the s-wave scattering $U_s = 4\pi\hbar^2 a/m \int n^2(r)d^3r$, and the second one is due to the on-site dipole-dipole interaction $U_{\text{dip}} = 1/(2\pi) \int \widetilde{U}_{\text{dd}}(q)\tilde{n}^2(q)d^3q$, being $\widetilde{U}_{\text{dd}}(q)$ and $\tilde{n}(q)$ the Fourier transform of the dipole potential and density, respectively [54].

Because of the localisation of the wavefunctions at the bottom of the optical lattice wells, the long range part of the dipole-dipole interaction $U_{\vec{\ell}}$ is in a very good approximation given by the dipole-dipole interaction potential at distance $\vec{\ell}$, $U_{\vec{\ell}} = (C_{\text{dd}}/4\pi)[1 - 3\cos^2(\theta_{\vec{\ell}})]/\ell^3$ multiplied by the densities n_i and n_j in the two sites, where the quantity C_{dd}, proportional to the dipole moment squared, has been defined Sect.2.2 and $\theta_{\vec{\ell}}$ is the angle between $\vec{\ell}$ and the orientation of the dipoles (see Fig.1).

The ratio between the total on-site interaction $U = U_s + U_{\text{dip}}$ and the nearest neighbour dipolar interaction U_{NN} determines much of the physics of the system. As we mentioned previously, in order to make the effects of long-range interactions observable it might be necessary to have a not too small ratio U/U_{NN}. It can be varied by tuning the strength and the sign of the on-site dipole-dipole interaction U_{dip} by changing the anisotropy of the Wannier functions at the bottom of the lattice sites, as depicted in Fig.11. In standard experiments with ^{52}Cr, $U/U_{NN} \approx 400$ (for $\varepsilon_{\text{dd}} = \mu_0(6\mu_B)^2 m/(12\pi\hbar^2 a) \approx 0.158$ and spherical localisation at the bottom of the potential well at $s = 20E_R$, where E_R is the recoil energy at $\lambda = 500$ nm). Using a Feshbach resonance to change the s-wave scattering length, as recently demonstrated with Chromium atoms [18], U/U_{NN} can be virtually tuned down to zero.

$$U_{dip} < 0 \qquad U_{dip} = 0 \qquad U_{dip} > 0$$
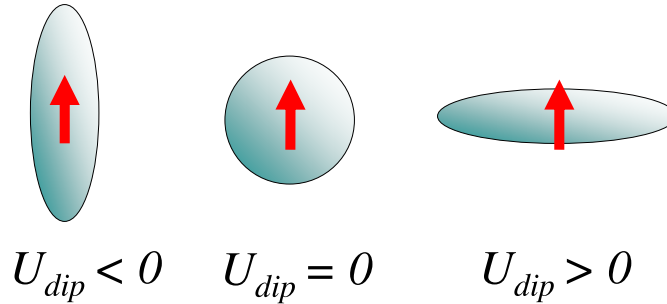
FIGURE 11. On-site dipole-dipole interaction U_{dip} depending on the anisotropy of the wavefunction at the bottom of the lattice wells. For vertically pointing dipoles, the dipole-dipole interaction is mainly attractive for cigar-shaped wells (left), vanishes for spherical wells (center) and is mainly repulsive for pancake-shaped wells (right).

Analogously as before, a time dependent variational principle leads to the dynamical equations for the Gutzwiller coefficients which now include a contribution due to the long-range part of the interaction

$$i\frac{d f_n^{(i)}}{dt} = -J\left[\bar{\varphi}_i\sqrt{n_i}f_{n-1}^{(i)}+\bar{\varphi}_i^*\sqrt{n_i+1}f_{n+1}^{(i)}\right]+ \tag{41}$$

$$+ \left[\frac{U}{2}n_i(n_i-1)+\sum_{\vec{\ell}}U_{\vec{\ell}}\,\bar{n}_{i,\vec{\ell}}\,n_i-\mu n_i\right]f_n^{(i)},$$

with $\bar{n}_{i,\vec{\ell}}=\sum_{\langle j\rangle_{i,\vec{\ell}}}n_j$.

The imaginary time evolution, which mimics dissipation in the system, converges unambiguously to the ground state of the system for the Bose-Hubbard model in presence of on-site interaction only. In the presence of long-range interaction it shows a strikingly different behaviour and converges often to different configurations, depending on the exact initial conditions. In this way, we clearly get a feeling of the existence of metastable states in the system. In the real time evolution, their stability is confirmed by typical small oscillations around a local minimum of the energy.

5.1.1. Conditions to have an insulating lobe

The existence of metastable stationary states can be confirmed using the mean-field perturbative approach introduced in Sect.4.1.2. In this section we will generalise it to include long-range interaction and we show that, beyond the ground state lobe, insulating lobes for the metastable states exist [19].

The first important difference is that in the limit $\beta \to \infty$, the system can populate any local minimum of the energy and not necessarily the ground state, as it was before. Hence, the partition function becomes

$$\mathscr{L} \equiv \mathscr{Z}_{MS} = e^{-\beta E_{MS}}, \tag{42}$$

where MS indicates any of the metastable states, whose existence we are for the moment assuming and going to demonstrate in the following.

The expectation value of the order parameter reads, similarly to before

$$\varphi_i = J\bar{\varphi}_i e^{\beta E_{MS}}\int_0^\beta Tr\left[\hat{a}_i e^{-(\beta-\tau)H_0}\hat{a}_i^\dagger e^{-\tau H_0}\right]d\tau, \tag{43}$$

where H_0 now includes also the dipole-dipole interaction

$$H_0 = \sum_i\left[\frac{U}{2}n_i(n_i-1)-\mu n_i+\sum_{\vec{\ell}}U_{\vec{\ell}}\,\bar{n}_i\left(n_i-\frac{\langle n_i\rangle}{2}\right)\right]. \tag{44}$$

On the other hand, the tunneling part H_J has not changed with respect to the case of zero-range interaction.

It is important to stress at that point that in order to investigate the stability of a given metastable state, the trace is performed on the subspace of states differing from it only by small perturbations. Specifically this means that we take into account only those states which differ from the metastable state by adding or removing one particle.

The derivation follows the one presented in Sect.4.1.2. The important analogies and differences are summarised here:

a) the ground state is replaced by any metastable state and only small perturbations around that metastable state are considered;

b) the assumption of metastability of a given configuration has to ensured by checking that all the states obtained from the metastable state $|MS\rangle$ by adding or removing one particle at *any* of the lattice sites j have higher energy than E_{MS}, i.e.

$$E_{MS} - H_0^{|\Phi\rangle} \leq 0, \quad \text{for } |\Phi\rangle = |MS \pm 1, j\rangle \; \forall j; \tag{45}$$

c) the only non vanishing contributions arise, analogously to Eq.(36), from the terms where

$$
\begin{aligned}
&1) \quad |\Phi\rangle \text{ is the metastable state } \text{ or} \\
&2) \quad |\Phi + 1, i\rangle \text{ is the metastable state, i.e. } |\Phi\rangle \text{ is the state} \\
&\qquad \text{obtained by removing one particle from the metastable state at site } i.
\end{aligned}
\tag{46}
$$

These are exactly the same criteria as for on-site interaction only, a crucial difference being that now the atomic distribution in the lattice sites might be not uniform so that the effect of adding and removing one particle at *all* lattice sites has to be considered to ensure condition (45) above. Taking the case of dipole-dipole interaction explicitly into account, one gets that for all i the conditions

$$U(n_i - 1) < \mu - V_{dip}^{1,i} < U n_i \tag{47}$$

have to be satisfied, implying for the boundary of the lobes at $J = 0$ the values

$$\mu_{min} = \max_i \left[U(n_i - 1) + V_{dip}^{1,i} \right], \tag{48}$$

$$\mu_{max} = \min_i \left[U n_i + V_{dip}^{1,i} \right], \tag{49}$$

where $V_{dip}^{1,i}$ is the dipole-dipole interaction of 1 atoms at site i with the rest of the lattice. Clearly in the absence of dipole-dipole interaction, these conditions reduce to the ones written in Eq.(20).

Those stability conditions immediately lead us to draw two important conclusions:

i) configurations with no integer filling factor can be stable as soon as one nearest neighbour is included in the interaction (see Fig.12(a));
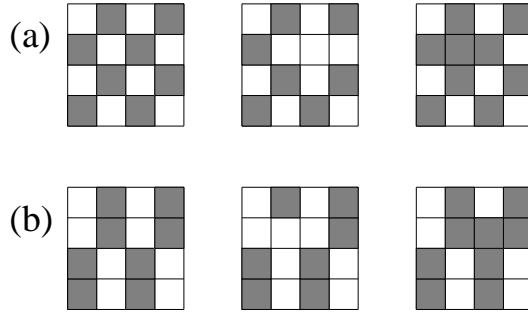
FIGURE 12. (a) Sketch of a checkerboard Mott insulating phase with energy $E(GS)$ (left); configuration where 1 atom has been removed with energy $E(GS, -1, i) = E(n = 1) + \mu$ (center); configuration where 1 atom has been added with energy $E(n = 1, +1, i) = E(n = 1) - \mu + 4U_{NN}$ (right). For $0 < \mu < 4U_{NN}$, the Mott $n = 1$ phase is the ground state. (b) Sketch of a metastable Mott insulating phase at filling factor $1/2$ with energy $E(MS)$ (left); configuration where 1 atom has been removed with energy $E(MS, -1, i) = E(n = 1) + \mu - U_{NN}$ (center); configuration where 1 atom has been added with energy $E(n = 1, +1, i) = E(n = 1) - \mu + 3U_{NN}$ (right). For $U_{NN} < \mu < 3U_{NN}$, this metastable state is stable. For the sake of simplicity, in those examples we have considered only one nearest neighbour in the dipole-dipole interaction.

ii) for a given chemical potential there exist configurations at higher energy compared to the ground state which also fulfill the stability condition (see Fig.12(b)). We call such configurations *metastable states*.

The explicit expression for the order parameter now reads

$$\varphi_i = \bar{\varphi}_i J \left[\frac{n_i + 1}{U n_i - \mu + V_{dip}^{1,i}} - \frac{n_i}{U(n_i - 1) - \mu + V_{dip}^{1,i}} \right].$$ (50)

Equation (50) is a system of linear equations in the variables φ_i described by the matrix M: $M\vec{\varphi} = 0$. When $det(M) \neq 0$, this equation only allows the trivial solution $\varphi_i = 0 \; \forall i$, implying that the system is in a Mott insulating phase. On the other hand, if $det(M) = 0$, it is possible to have $\varphi_i \neq 0$, implying that the system has become superfluid.

Due to the non homogeneity of the solution in the presence of long-range interaction this is a system of linear equations whose dimension depends on the size of the lattice. In practise we can access with this method lattice sizes of the order of 20-30 lattice sites per direction.

5.1.2. *Phase diagram for long-range interactions*

The phase diagram of the system is shown in Fig.13. As predicted by the perturbative mean-field approach presented in the previous section, in the presence of long-range interactions, there are insulating lobes corresponding both to ground and metastable states and to integer and non integer filling factors. In particular non uniform distributions of the atoms are allowed.
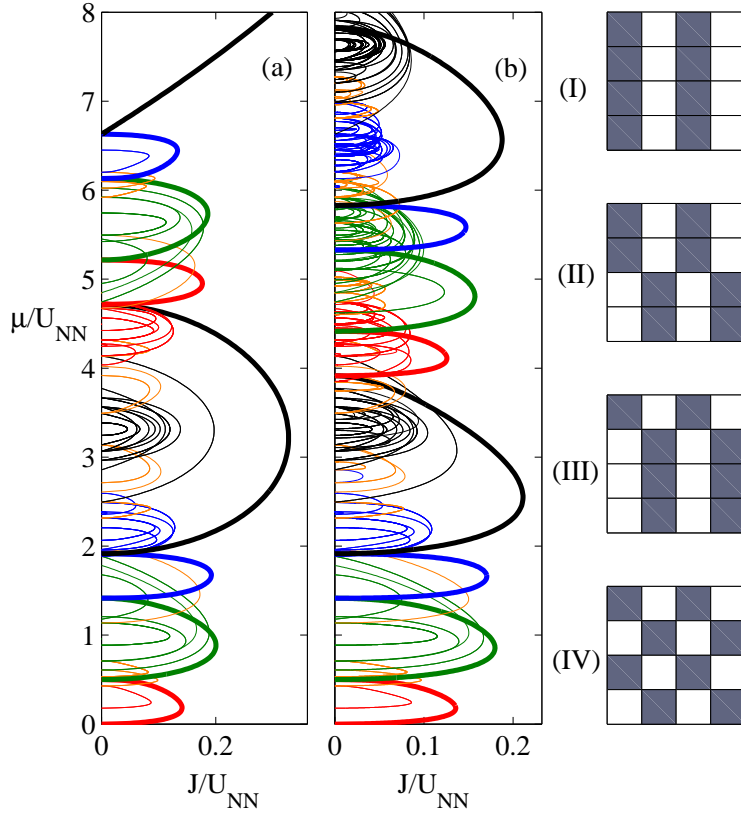
FIGURE 13. Phase diagram for weak and strong dipole-dipole interaction and interaction range up to the 4th nearest neighbour: $U/U_{NN} = 20$ (a) and $U/U_{NN} = 2$ (b). The thick lines are the ground state lobes, found (for increasing chemicals potential) for filling factors equal to all multiples of $1/8$. The thin lines are the metastable states, found at filling factors equal to multiples of $1/16$. Some of the metastable configurations at filling factor $1/2$ (I to III) and corresponding ground state (IV). Empty sites are light and sites occupied with 1 atom are dark. Figure from [19].

The phase diagram in Fig.13 has been calculated for an interaction range of four nearest neighbours, as shown in Fig.10. For this specific range of interaction, the lowest filling factor allowed is $1/8$.

By increasing the relative strength the long-range interaction with respect to the on-site one, the lobes corresponding to fractional filling factors become comparable to the ones relative of the standard Mott phase with commensurate filling (cfr. Fig.13(b) with Fig.13(a), where the upper lobe for $n = 1$ is only partially shown).

This phase diagram is confirmed by the imaginary and real time evolution of the system: depending on the initial conditions the imaginary time evolution can converge to the metastable configurations, while in the real time evolution, their stability is reflected into typical small oscillations around a local minimum of the energy. In the next section we discuss the lifetime of the metastable states, connected to the possibility of tunneling between different local minima of the energy landscape.

5.2. Stability of the metastable states

We study the stability of the metastable states with a path integral formulation in imaginary time [55], which can describe the tunneling below a potential barrier (instanton effect). The path integral representation for the propagator in imaginary time takes the form

$$\int \mathscr{D}[\Phi^*,\Phi] \prod_{j=1}^{N} \langle \Phi_j | e^{-H\Delta\tau} | \Phi_{j-1} \rangle \approx \int \mathscr{D}[\Phi^*,\Phi] e^{-\int \mathscr{L}(\tau,\Phi,\dot{\Phi})d\tau}, \qquad (51)$$

which gives the following expression for the Lagrangian $\mathscr{L} = \langle \Phi | \dot{\Phi} \rangle - H$. With the substitution $\Phi = (x+ip)/\sqrt{2}$ and $\Phi^* = (x-ip)/\sqrt{2}$, the Lagrangian becomes $\mathscr{L} = -ip\dot{x} + H$. This can be put in the canonical form $\mathscr{L} = P\dot{X} - \tilde{H}(X,P)$ by defining the new coordinates $X = x$ and $P = \partial\mathscr{L}/\partial\dot{X} = -ip$. In those new coordinates, the Hamiltonian governing the dynamics in imaginary time is

$$\tilde{H}(X,P) = -H(p(P),X) = \frac{P^2}{2m} - V(X). \qquad (52)$$

For this reason, the dynamics in imaginary time, describing the instanton effect between two potential wells, is said to happen in the inverted potential $-V(X)$, as depicted in Fig.14.

FIGURE 14. Tunneling of a particle in a double-well potential (left); in imaginary time, this tunneling event (instanton) is described by the dynamics in the inverted potential (right).

We exploit this formalisms to describe the tunneling between the different metastable configurations found in the previous section. In order to reduce our problem to the dynamics of a single variable X and its conjugate momentum P, we make a variational Ansatz on the Gutzwiller wavefunction which parametrises the population of the lattice well from 1 to 0 and viceversa.
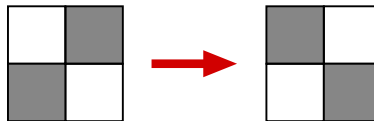
FIGURE 15. Transition from a checkerboard configuration to its opposite one, where full sites are replaced by empty sites and viceversa.

Here we present in particular the results for the transition between one configuration (in the specific case, the checkerboard) and its opposite one, where full and empty wells have been interchanged, as shown in Fig.15. For this transition, the tunneling time is $\omega_0 T \approx \exp[S_0]$, where ω_0 is the typical oscillation frequency around the minimum of the energy. The tunneling time diverges for $J \to 0$ and roughly scales like $\omega_0 T \approx \exp[N_s \hbar] \exp[-N_s \hbar J/\tilde{J}]$ for $J/\tilde{J} > 0.3$, as shown in Fig.16.
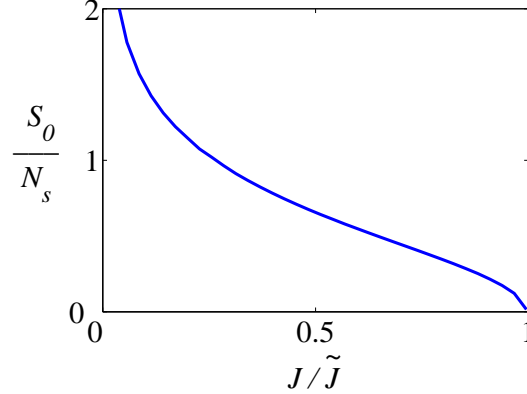
FIGURE 16. Action S_0 for the transition described in Fig.15, calculated with a variational Ansatz for the path integral formalisms in imaginary time. The lifetime of the tunneling event is given by $\omega_0 T \approx \exp[S_0]$. N_s is the number of sites which invert their population in the transition and $\tilde{J}$ is of the order of the tip of the insulating lobe.

This analysis suggests that the metastable configurations are very stable when many sites must invert their population to reach another metastable state. However, one should not forget that especially in larger lattices two metastable configurations might differ just by the occupation of few lattice sites. This, and the corresponding small energy difference, should be carefully taken into account in a realistic analysis at finite temperature.


5.3. Initialisation and detection

Very important issues are the initialisation and detection of the atomic states in the lattice. One can use superlattices in order to prepare the atoms in configurations of preferential symmetry. This idea is presently pursued by several experimental groups [56]. We have checked that the presence of defects is strongly reduced when a local potential energy following desired patterns is added to the optical lattice. Note that the configurations obtained in such a way will also remain stable once the superlattice is removed, thanks to dipole-dipole interaction.

The spatially modulated structures created in such a way can be detected via the measurement of the noise correlations of the expansion pictures [42, 57, 58]: the ordered structures in the lattice give rise to different patterns in the spatial noise correlation function

$$C(d) = \frac{\int \langle n_{TOF}(x+d/2) n_{TOF}(x-d/2) \rangle \, d^2 x}{\int \langle n_{TOF}(x+d/2) \rangle \langle n_{TOF}(x-d/2) \rangle \, d^2 x} \approx \sum_{k,\ell} e^{i(m/\hbar t)d(r_k - r_\ell)} n_k n_\ell = |\mathscr{F}(n)|^2$$

equal to the modulus square of the Fourier transform of the density distribution in the lattice (n_{TOF} is the density distribution after time of flight, while n_k is the density distribution in the lattice). Such a measurement is in principle able to recognise the defects in the density distribution, which could be exactly reconstructed starting from the patterns in the spatial noise correlation function. For the moment, the signal to noise ratio required for single defect recognition is beyond the present experimental possibilities. However, averaging over a finite number of different experimental runs producing the same spatial distribution of atoms in the lattice, a good signal can be obtained. In Fig.17, we show the noise correlations for the metastable configurations at filling factor $1/2$ shown in Fig.13.
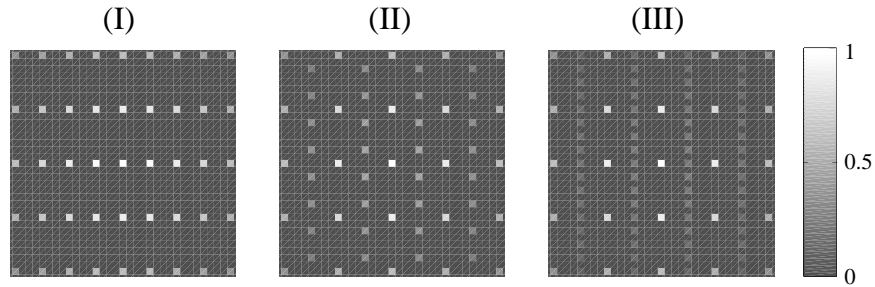
FIGURE 17. Spatial noise correlation patterns for configurations (I) to (III) in Fig. 13, assuming a localised gaussian density distribution at each lattice site. Figure from [19].

Presently we are studying the possibility of transferring in a controlled way those systems from one configuration to another [53]. This, together with the capability of initialising and reading out the state of the lattice, might make those systems useful for applications as quantum memories.

6. CONCLUSIONS

In this paper, we have given a review of some aspects of the physics of ultra-cold atomic gases interacting via a long-range dipolar potential. On the experimental side, we have presented an overview of the state of the art of the experiments, starting from the first observation of dipolar effects in a Chromium Bose-Einstein condensate to the most recent experiments demonstrating strong dipolar interactions in those systems. The description of those experimental achievements has been accompanied by the explanation of the underlying theoretical models. On the theoretical side, we have presented our recent results on dipolar gases in optical lattices, describing the theoretical framework and explaining in a detailed way the difference brought in by long-range interactions compared to the case of zero-range interactions. In particular, we have pointed out that long-range interactions introduce a huge number of metastable states in the system, which are not present in the case of zero-range interaction. We have motivated why Chromium atoms are the best candidates at the moment for the realisation of such systems. We hope that with our work, we have drawn the attention of the statistical mechanics community devoted to the study of long-range interactions to this novel kind of systems and that this will be source of inspiration for future collaborations.

ACKNOWLEDGMENTS

REFERENCES

1. H.M. Anderson, J.R. Ensher, M.R. Matthews, C.E. Wieman, and E.A. Cornell, Science **269**, 198 (1995); C.C. Bradley, C.A. Sackett, J.J. Tollett, and R.G. Hulet, Phys. Rev. Lett. **75**, 1687 (1995); K.B. Davis, M.-O. Mewes, M.R. Andrews, N.J. van Druten, D.S. Durfee, D.M. Kurn, and W. Ketterle, Phys. Rev. Lett. **75**, 3969 (1995).
2. B. DeMarco and D.S. Jin, Science **285**,1703 (1999).
3. D.S. Jin, J.R. Ensher, M.R. Matthews, C.E. Wieman, and E.A. Cornell, Phys. Rev. Lett. **77**, 420 (1996); M.-O. Mewes, M.R. Andrews, N.J. van Druten, D.M. Stamper-Kurn, D.S. Durfee, C.G. Townsend, and W. Ketterle, Phys. Rev. Lett. **77**, 988 (1996).
4. M.R. Andrews, C.G. Townsend, H.J. Miesner, D.S. Durfee, D.M. Kurn, and W. Ketterle, Science **275**, 637 (1997).
5. see e.g. B.P Anderson and M.A. Kasevich, Science **282**, 1686 (1998); I. Bloch, T.W. Hänsch, and T. Esslinger, Phys. Rev. Lett. **82**, 3008 (1999); E.W. Hagley, L. Deng, M. Kozuma, J. Wen, K. Helmerson, S.L. Rolston, and W.D. Phillips, Science **283**, 1706 (1999).
6. L. Deng, E.W. Hagley, J. Wen, M. Trippenbach, Y. Band, P.S. Julienne, J.E. Simsarian, K. Helmerson, S.L. Rolston, and W.D. Phillips, Nature **398**, 218 (1999).
7. S. Burger, K. Bongs, S. Dettmer, W. Ertmer, K. Sengstock, A. Sanpera, G. V. Shlyapnikov, and M. Lewenstein, Phys. Rev. Lett. **83**, 5198 (1999); J. Denschlag, J.E. Simsarian, D.L. Feder, C.W. Clark, L.A. Collins, J. Cubizolles, L. Deng, E.W. Hagley, K. Helmerson, W.P. Reinhardt, S.L. Rolston, B.I. Schneider, W.D. Phillips, Science **287**, 97 (2000).
8. M.R. Andrews, D.M. Kurn, H.-J. Miesner, D.S. Durfee, C.G. Townsend, S. Inouye, and W. Ketterle, Phys. Rev. Lett. **79**, 553 (1997).
9. O.M. Maragò, S.A. Hopkins, J. Arlt, E. Hodby, G. Hechenblaikner, and C.J. Foot, Phys. Rev. Lett. **84**, 2056 (2000).
10. M.R. Matthews, B.P .Anderson, P.C. Haljan, D.S. Hall, C.E. Wieman, and E.A. Cornell, Phys. Rev. Lett. **83**, 2498 (1999); K.W. Madison, F. Chevy, W. Wohlleben, and J. Dalibard, Phys. Rev. Lett. **84**, 806 (2000); J.R. Abo-Shaeer, C. Raman, J.M. Vogels, and W. Ketterle, Science **292**, 476 (2001).
11. P. Courteille, R.S. Freeland, D.J. Heinzen, F.A. van Abeelen, and B.J. Verhaar, Phys. Rev. Lett. **81**, 69 (1998); S. Inouye, K.B. Davis, M.R. Andrews, J. Stenger, H.-J. Miesner, D.M. Stamper-Kurn, and W. Ketterle, Nature **392**, 151 (1998).
12. M. Greiner, O. Mandel, T. Esslinger, T.W. Hänsch, and I. Bloch, Nature **415**, 39 (2002).
13. Z. Hadzibabic, P. Krüger, M. Cheneau, B. Battelier, and J. Dalibard, Nature **441**, 1118 (2006).
14. T.T. Kinoshita, T. Wenger and D.S. Weiss, Science **305**, 1125 (2004); B. Paredes, A. Widera, V. Murg, O. Mandel, S. Fölling, I. Cirac, G.V. Shlyapnikov, T.W. Hänsch and I. Bloch, Nature **429**, 277 (2004).
15. due to the large number of experimental and theoretical papers on this subject, we address the reader to the recent review [24].
16. see C. Ospelkaus, S. Ospelkaus, L. Humbert, P. Ernst, K. Sengstock, and K. Bongs, Phys. Rev. Lett. **97**, 120402 (2006) and references therein.
17. M. Baranov, Ł. Dobrek, K. Góral, L. Santos, and M. Lewenstein, Physica Scripta **102**, 74 (2002).
18. T. Lahaye, T. Koch, B. Frölich, M. Fattori, J. Metz, A. Griesmaier, S. Giovanazzi, and T. Pfau, Nature **448**, 672 (2007).
19. C. Menotti, C. Trefzger, and M. Lewenstein, Phys. Rev. Lett. **98**, 235301 (2007).
20. F.S. Dalfovo, S. Giorgini, L.P. Pitaevskii, and S. Stringari, Rev. Mod. Phys. **71**, 463 (1999).
21. L. . Pitaevskii and S. Stringari, *Bose-Einstein condensation*, (Clarendon Press, Oxford, 2003).

22. C. Pethick and H. Smith, *Bose-Einstein Condensation in Dilute Gases* (Cambridge University Press, 2002).

23. I. Bloch, J. Dalibard, and W. Zwerger, arXiv:0704.3011.

24. S. Giorgini, L.P. Pitaevskii, and S. Stringari, arXiv:0706.3360.

25. Special Issue *Ultracold Polar Molecules: Formation and Collisions*, Ed. J. Doyle, B. Friedrich, R.V. Krems, and F. Masnou-Seeuws, Eur. Phys. J. D **31** No.2, (2004).

26. T.F. Gallagher, *Rydberg Atoms* (Cambridge University Press, 1994); D. Tong, S.M. Farooqi, J. Stanojevic, S. Krishnan, Y.P. Zhang, R. Côté, E.E. Eyler and P.L. Gould, Phys. Rev. Lett. **93**, 063001 (2004); T. Vogt, M. Viteau, J. Zhao, A. Chotia, D. Comparat and P. Pillet, Phys. Rev. Lett. **97**, 0803003 (2006); R. Heidemann, U. Raitzsch, V. Bendkowsky, B. Butscher, R. Löw, L. Santos, and T. Pfau, Phys. Rev. Lett. **99**, 163601 (2007).

27. J. Stuhler, A. Griesmaier, T. Koch, M. Fattori, T. Pfau, S. Giovanazzi, P. Pedri, and L. Santos, Phys. Rev. Lett. **95**, 150406 (2005).

28. A. Griesmaier, J. Phys. B **40**, 91 (2007).

29. P.O. Schmidt, S. Hensler, J. Werner, T. Binhammer, A. Görlitz and T. Pfau, J. Opt. B: Quantum Semiclass. Opt. **5**, 170 (2003).

30. P.O. Schmidt, S. Hensler, J. Werner, T. Binhammer, A. Görlitz and T. Pfau, J. Opt. Soc. Am. B **20**, 5 (2003).

31. S. Hensler, J. Werner, A. Griesmaier, P.O. Schmidt, A. Görlitz, T. Pfau, S. Giovanazzi and K. Rzążewski, Appl. Phys. B **77**, 765 (2003).

32. A. Griesmaier, J. Werner, S. Hensler, J. Stuhler and T. Pfau, Phys. Rev. Lett. **94**, 160401 (2005).

33. J. Werner, A. Griesmaier, S. Hensler, J. Stuhler, T. Pfau, A. Simoni and E. Tiesinga, Phys. Rev. Lett. **94**, 183201 (2005).

34. L. Santos, G. Shlyapnikov, and M. Lewenstein, Phys. Rev. Lett. **90**, 250403 (2003); see also D.H. O'Dell, S. Giovanazzi, and G. Kurizki, Phys. Rev. Lett. **90**, 110402 (2003).

35. C. Eberlein, S. Giovanazzi, and D.H.J. O'Dell, Phys. Rev. A **71**, 033618 (2004); S. Giovanazzi, P. Pedri, L. Santos, A. Griesmaier, M. Fattori, T. Koch, J. Stuhler, and T. Pfau, Phys. Rev. A **74**, 013621 (2006).

36. Y. Castin and R. Dum, Phys. Rev. Lett. **77**, 5315 (1996); Yu. Kagan, E. L. Surkov, and G. V. Shlyapnikov, Phys. Rev. A **54**, R1753 (1996).

37. M.P.A. Fisher, P.B. Weichman, G. Grinstein, and Daniel S. Fisher, Phys. Rev. B **40**, 546 (1989).

38. D. Jaksch, C. Bruder, J.I. Cirac, C.W. Gardiner, and P. Zoller, Phys. Rev. Lett. **81**, 3108 (1998).

39. K. Góral, L. Santos and M. Lewenstein, Phys. Rev. Lett. **88**, 170406 (2002).

40. D.L. Kovrizhin, G.V. Pai, and S. Sinha, Europhys. Lett. **72**, 162 (2005).

41. P. Sengupta, L.P. Pryadko, F. Alet, M. Troyer, and G. Schmid, Phys. Rev. Lett. **94**, 207202 (2005).

42. V.W. Scarola, E. Demler, and S. Das Sarma, Phys. Rev. A **73**, 051601(R) (2006).

43. E. Kim and M.H.W. Chan, Nature **427**, 225 (2004); Science **305**, 1941 (2004); Phys. Rev. Lett. **97**, 115302 (2006); S. Sasaki, F. Caupin, and S. Balibar, arXiv:0707.3110.

44. N.W. Ashcroft and N.D. Mermin, *Solid State Physics* (Saunders College Publishing, 1976).

45. K. Sheshadri, H. R. Krishnamurthy, R. Pandit, and T.V. Ramakrishnan, Europhys. Lett. **22**, 257 (1993).

46. Subir Sachdev, *Quantum Phase Transitions* (Cambridge University Press, 1999).

47. J.K. Freericks and H. Monien, Europhys. Lett. **26**, 545 (1994); Phys. Rev. B **53**, 2691 (1996).

48. see e.g. R.T. Scalettar, G.G. Batrouni, and G.T. Zimanyi, Phys. Rev. Lett. **66**, 3144; W. Krauth, N. Trivedi, and D. Ceperley, Phys. Rev. Lett. **67**, 2307 (1991); N.V. Prokofev, B.V. Svistunov, and I.S. Tupisyn, Phys. Lett. A **238**, 253 (1998).

49. G. G. Batrouni, V. Rousseau, R. T. Scalettar, M. Rigol, A. Muramatsu, P. J. Denteneer, and M. Troyer, Phys. Rev. Lett. **89**, 117203 (2002)

50. S. Fölling, A. Widera, T. Müller, F. Gerbier, I. Bloch, Phys. Rev. Lett. 97, 060403 (2006).

51. D. Jaksch, V. Venturi, J. I. Cirac, C. J. Williams, and P. Zoller, Phys. Rev. Lett. 89, 040402 (2002); J. Zakrzewski, Phys. Rev. A **71**, 043601 (2005).

52. D.-W. Wang, M.D. Lukin, and E. Demler, Phys. Rev. Lett. **97**, 180413 (2006).

53. C. Trefzger, C. Menotti and M. Lewenstein, in preparation.

54. K. Góral and L. Santos, Phys. Rev. A **66**, 023613 (2002).

55. X.-G. Wen, *Quantum field theory of many-body systems*, (Oxford University Press, Oxford, 2004).

56. P.J. Lee, M. Anderlini, B.L. Brown, J. Sebby-Strabley, W.D. Phillips, and J.V. Porto, Phys. Rev. Lett. **99**, 020402 (2007); and I. Bloch, J. Henker-Denschlag, private communications.

57. E. Altman, E. Demler, and M.D. Lukin, Phys. Rev. A **70**, 013603 (2004).

58. S. Fölling, F. Gerbier, A. Widera, O. Mandel, T. Gericke, and I. Bloch, Nature **434**, 481 (2005).